Water Splitting with Enhanced Efficiency Using a Nickel-Based Co-Catalyst at a Cupric Oxide Photocathode

Carmelo Lo Vecchio [1],*, Stefano Trocino [1], Giosuè Giacoppo [1], Orazio Barbera [1], Vincenzo Baglio [1], María I. Díez-García [2], Maxime Contreras [2], Roberto Gómez [2] and Antonino Salvatore Aricò [1]

1 Istituto di Tecnologie Avanzate per l'Energia "Nicola Giordano", Consiglio Nazionale delle Ricerche (CNR-ITAE), Via Salita Santa Lucia sopra Contesse 5, 98126 Messina, Italy; stefano.trocino@itae.cnr.it (S.T.); giosue.giacoppo@itae.cnr.it (G.G.); orazio.barbera@itae.cnr.it (O.B.); vincenzo.baglio@itae.cnr.it (V.B.); antonino.arico@itae.cnr.it (A.S.A.)

2 Departament de Química Física, Institut Universitari d'Electroquímica, Universitat d'Alacant, Apartat 99, E-03080 Alicante, Spain; mariaisabel.diez@ua.es (M.I.D.-G.); maxime.contreras@ua.es (M.C.); Roberto.Gomez@ua.es (R.G.)

* Correspondence: carmelo.lovecchio@itae.cnr.it; Tel.: +39-090-624-288

Abstract: Homemade non-critical raw materials such as Ni or NiCu co-catalysts were added at the photocathode of a tandem cell, constituted by photoelectrodes made of earth-abundant materials, to generate green solar hydrogen from photoelectrochemical water splitting. Oxygen evolving at the Ti-and-P-doped hematite/TCO-based photoanode and hydrogen at the cupric oxide/GDL-based photocathode are separated by an anion exchange polymer electrolyte membrane placed between them. The effect of the aforementioned co-catalysts was studied in a complete PEC cell in the presence of the ionomer dispersion and the anionic membrane to evaluate their impact under practical conditions. Notably, different amounts of Ni or NiCu co-catalysts were used to improve the hydrogen evolution reaction (HER) kinetics and the overall solar-to-hydrogen (STH) efficiency of the photoelectrochemical cells. At -0.6 V, in the bias-assisted region, the photocurrent density reaches about 2 mA cm^{-2} for a cell with 12 µg cm^{-2} of Ni loading, followed by 1.75 mA cm^{-2} for the cell configuration based on 8 µg cm^{-2} of NiCu. For the best-performing cell, enthalpy efficiency at -0.4 V reaches a first maximum value of 2.03%. In contrast, the throughput efficiency, which is a ratio between the power output and the total power input (solar + electric) provided by an external source, calculated at -1.225 V, reaches a maximum of 10.75%. This value is approximately three times higher than the best results obtained in our previous studies without the use of co-catalysts at the photocathode.

Keywords: low-cost semiconductors; tandem cell; cupric oxide photocathode; solar to hydrogen efficiency; photoelectrochemical cell; Ni-based co-catalysts

1. Introduction

Environmental emergencies that our planet is tackling, such as climatic change and global warming, result from the thoughtless employment of fossil fuels over past decades to satisfy the increasing world energy demand for supporting demographic, industrialization, and urbanistic growths [1,2]. Hydrogen fuel is characterized by a high mass–energy density (120–142 MJ/Kg); it is recognized as the most attractive "green" alternative to the dwindling supply of fossil fuels, such as gasoline (45 MJ/Kg), because its reaction, coupled with the oxygen reduction reaction occurring in a polymer electrolyte membrane fuel cell (PEMFC), gives the spontaneous formation of water and electricity without the release of pollutant gases. However, hydrogen formation from water splitting is a process requiring an external surplus of energy that could be provided by renewable and sustainable power sources, such as sunlight or wind [3–5].

In this field, the research on photoelectrochemical (PEC) water splitting (WS) relies on semiconductor electrodes (generally metal oxides) that exhibit appreciable photogenerated charge separation at the solid/liquid interface when illuminated by sunlight [6–9]. To the best of our knowledge, studies on photoelectrochemical cells were conducted, even recently [10–14], in a liquid electrolyte, thus requiring post-processing energy to separate evolved gas from water splitting. In our recent work, tandem photoelectrochemical cells were constituted by a solid polymeric membrane, acting as both gas separator and electrolyte, sandwiched between a photoanode and a photocathode [15–17].

As shown in Figure 1 and in our previous papers [18,19], an n-type Titanium-doped hematite photoanode is characterized by a dark orange color corresponding to a UV/vis absorption edge below 600 nm. The support, herein represented by a drilled transparent conductive oxide (TCO), is designed to permit both the water flow inside the scalable photoelectrochemical cell and the escape of the oxygen produced by water splitting. On the other side, light reaches the photocathode after passing through a yellow-hued anionic membrane. The CuO-based photocathode, characterized by a dark grey color, absorbs lower energy near-infrared (NIR) and visible light at wavelengths above 600 nm. Moreover, a gas diffusion layer (GDL) carbonaceous substrate, previously hydrophobized to avoid water flooding, was used to guarantee selective hydrogen escape from the electrode.
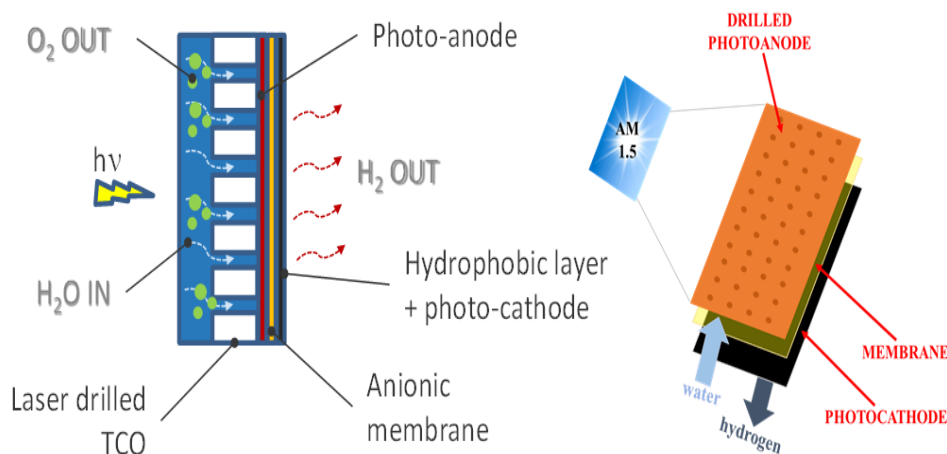
Figure 1. Sketch of reactants and products in a membrane-based photoelectrochemical tandem cell.

The working principle of a tandem cell relates to the generation of electron–hole pairs at the anode and the cathode, respectively, through the interaction with incoming light, as described in our previous studies [17–19]. In the Fe_2O_3-based photoanode, band edge bending drives photogenerated holes towards the electrolyte; the edge of its valence band (VB) is at a sufficiently high potential for triggering the evolution of oxygen from water. In the CuO-based photocathode, band bending drives photogenerated electrons towards the electrolyte; the edge of its conduction band (CB) is at a sufficiently low potential for the evolution of hydrogen from water. In the tandem cell architecture, all photons with energy above the narrower band gap, which should have a value close to 1 eV (1.25 eV for CuO), can contribute to the water-splitting process. The wide band gap oxide should possess a band gap in the range of 1.65 to 2.1 eV (2.1 eV for Fe_2O_3). The band gaps of CuO and Fe_2O_3 are adequate for capturing most of the solar spectrum; approximately 75% of the incoming light energy can be utilized.

The main drawbacks of PEC WS are derived from expensive electrode materials, with the complexity needed for achieving a high hydrogen purity, but with limited durability due to the employment of corrosive electrolytes and low solar to hydrogen (STH) efficiency [20–26].

Herein, we present a tandem PEC cell based on low-cost and non-critical raw materials such as iron oxide and copper oxide. A solid polymeric membrane is employed as the electrolyte and gas separator with very low hydrogen and oxygen crossover [19,27–29].

A liquid ionomer based on the same ammonium quaternary structure of the electrolyte is spread over the photoanode and photocathode. Particularly, Ni-based co-catalysts are deposited onto CuO/GDL to improve the hydrogen evolution reaction (HER) and the overall STH efficiency.

Among several semiconductor materials thoroughly investigated as candidates for the HER [30–32], p-type CuO was chosen to be employed as a photocathode. This choice relates to its low cost, low toxicity, proper band gap and band level position in relation to the reversible potential for hydrogen evolution, and good absorbance for the light transmitted through the photoanode and membrane [15,20]. However, this semiconductor exhibits low stability and limited efficiency [30,33]. To overcome these drawbacks, the introduction of co-catalysts, layered onto the CuO photocathode, appears to be a suitable strategy to enhance STH efficiency, thus improving the HER kinetics.

This study concerns a novel tandem cell architecture with a 0.25 cm^2 exposed area composed as reported in Figure 1 and focuses on the co-catalyst effect. To form a suitable n-type hematite semiconductor, Ti-doping [19] was adopted to increase the photo-response of the bare α-Fe$_2$O$_3$/TCO. The GDL-based-CuO photocathode was optimized in our previous study [18], achieving greater efficiency than that obtained with TCO-based electrodes (conductive glass). Herein, the investigated Ni and NiCu co-catalysts were prepared in-house, and their characteristics were evaluated in comparison with the bare materials used to fabricate the PEC cell.

2. Results

2.1. Physicochemical Characterization

2.1.1. X-ray Diffraction (XRD) of In-House-Prepared Co-Catalysts

Figure 2 shows the XRD physicochemical analysis of Ni and NiCu (1:1 wt%), in which the JCPDS card of Ni was used for the identification of the peaks. The NiCu alloy was characterized by a 1:1 weight ratio. A face-centered cubic (fcc) phase, corresponding to peaks and Miller indices at 44.4° (111), 51.7° (200), 76.4° (220), 92.3° (311), and 98.5° (222), characterized the structure of the metal nanoparticles in both catalysts and the crystallite sizes, as calculated by the Debye–Scherrer equation, were found to be 40 nm and 8 nm for Ni and NiCu species, respectively.
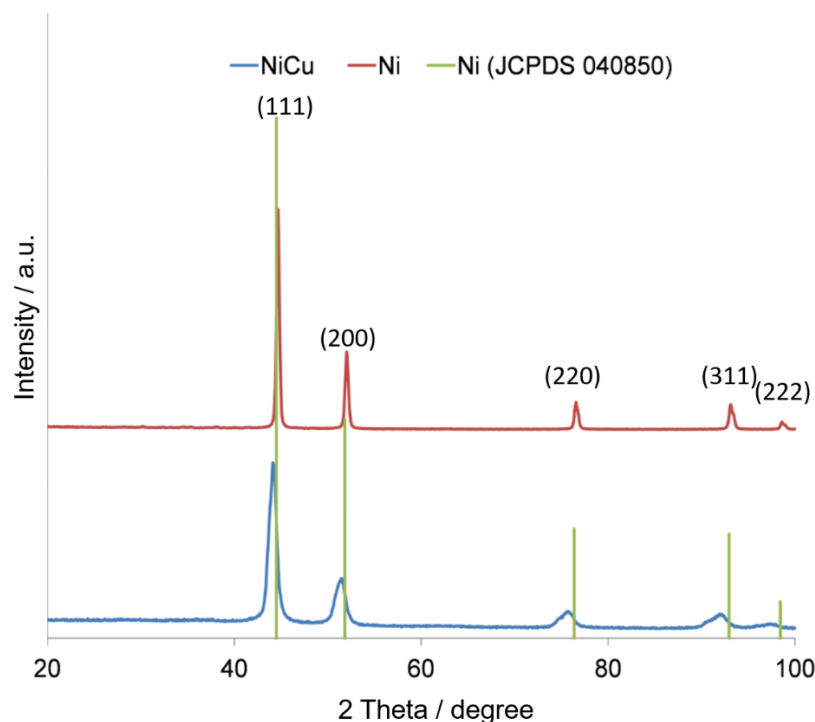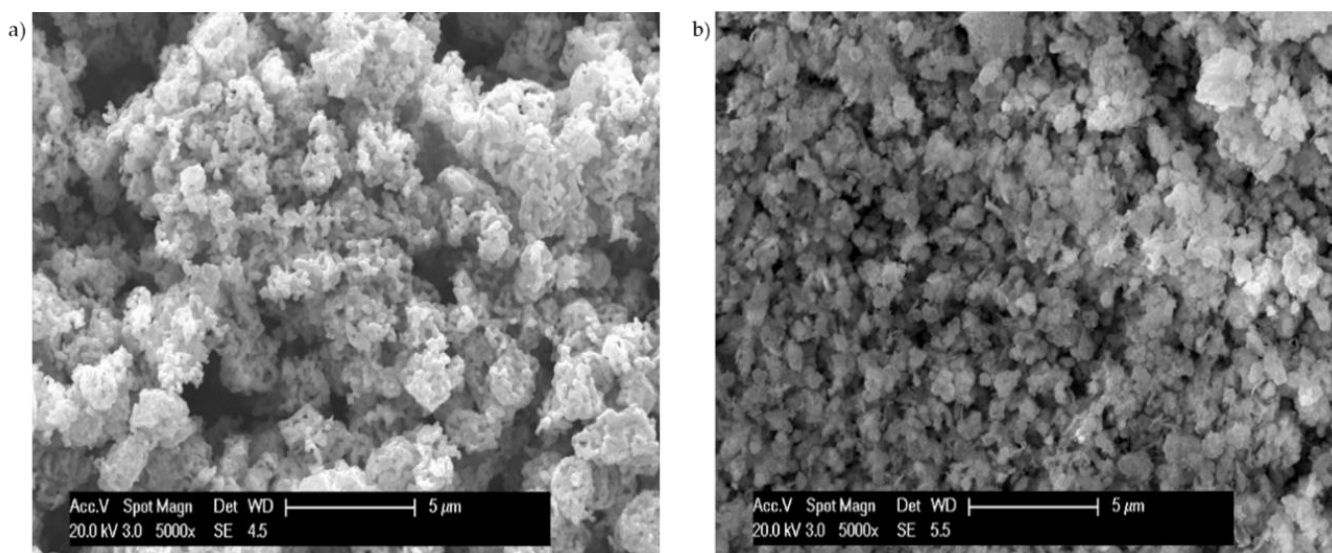

Figure 2. XRD patterns of in-house-synthesized Ni and NiCu catalysts.

The crystalline size is different due to the different temperatures used for the reduction of the respective oxides: 400 °C for the NiO powder and 300 °C for the NiCuOx alloy.

2.1.2. Morphological Characterization

Scanning electron microscopy (SEM) images for Ni (Figure 3a) and NiCu (Figure 3b) are shown at low magnification in Figure 3. Both images show quasi-spherical particles with significant agglomeration.

**Figure 3.** SEM images of in-house-synthesized Ni (**a**) and NiCu (**b**) catalysts.

2.2. Electrochemical Tests

Co-Catalyst at the CuO-Based Photocathode

Polarization tests were carried out in a PEC cell composed of Ti-and-P-doped hematite deposited over TCO glass, an anionic FAA-3 membrane electrolyte, and a photocathode formed by cupric oxide over hydrophobized (with 7% FEP, fluorinated ethylene propylene) Sigracet 35BC substrate, onto which metallic Ni or NiCu co-catalysts were deposited by drop-casting to investigate the effect of different metal loadings (8, 12 μg cm^{-2}). Thereafter, the annealing of CuO+Ni/GDL at 300 °C for 1 h was adopted to prevent the detachment of metal particles.

Before experiments, 25 μL cm^{-2} ionomer loading was deposited over the electrodes to guarantee a good interaction between photoelectrodes and the membrane. Furthermore, ionomer deposition creates a protective layer to enhance the durability of both CuO and the overall PEC. Finally, the photoanode, electrolyte, and photocathode were treated in a 1 M KOH solution for 1 h to facilitate the anion exchange process.

Polarization curves illustrated in Figure 4 were carried out in the dark (dashed lines) and under illumination (continuous lines). Figure 4a shows the behavior of the four PECs without a co-catalyst addition and with different amounts of co-catalysts at the photocathode between OCP and −0.6 V. Figure 4b displays the current density between OCP and −1.3 V in the bias-assisted region. Loadings of 8 or 12 μg cm^{-2} were used for metallic Ni, and a loading of 8 μg cm^{-2} was tested for the NiCu alloy in order to compromise between being cost-effective and optimizing performance for PEC cells.
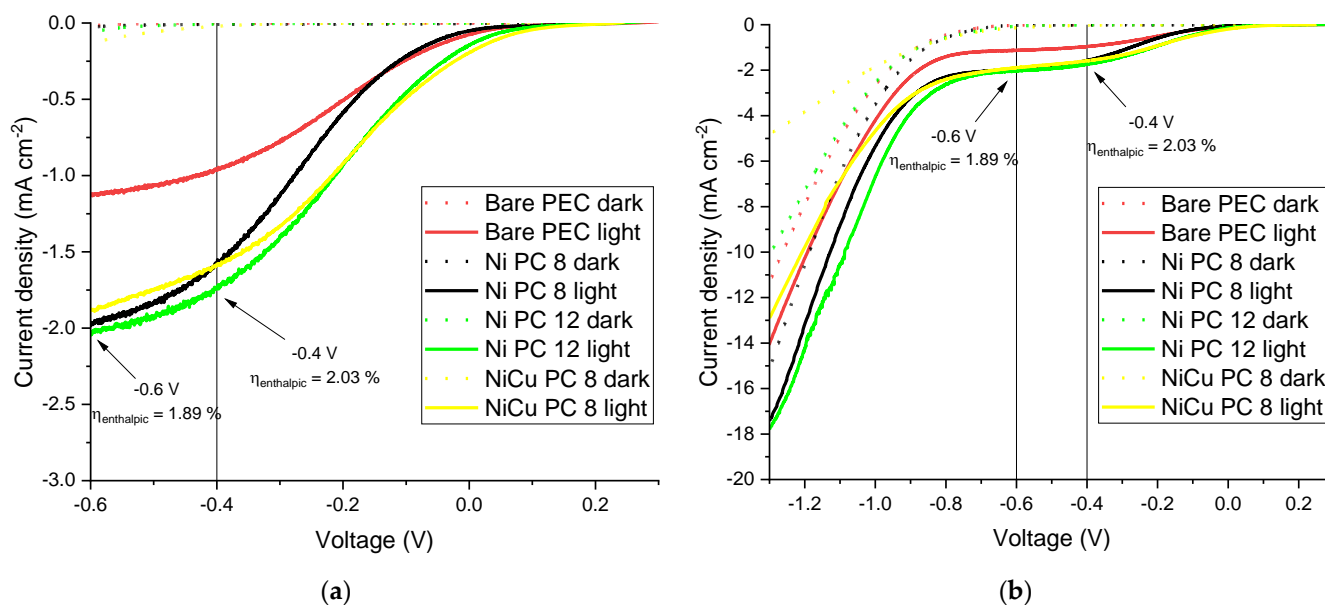
Figure 4. Polarization curves in the dark and under illumination from (**a**) OCP to –0.6 V bias-assisted region and (**b**) from 0.3 to –1.3 V.

The bare PEC, without a co-catalyst, was investigated for the sake of comparison, and was characterized by a lower value of the photocurrent density (difference between current density under illumination and in the dark) than those obtained with a Ni co-catalyst-based PEC. From Figure 4a, in the bias-assisted region at −0.4 V, the photocurrent density was −0.96, −1.57, and −1.73 mA cm^{-2} for the bare PEC and for PECs loaded with 8 and 12 μg cm^{-2} of Ni co-catalysts, respectively, and −1.56 mA cm^{-2} for the NiCu-based cell. At −0.6 V, the photocurrent density shows a similar value for the PECs based on 8 and 12 μg cm^{-2} (about 2 mA cm^{-2}) of Ni loading followed by 1.75 mA cm^{-2} for the PEC based on 8 μg cm^{-2} of NiCu. From Figure 4b, the photocurrent density below −0.6 V is affected by the different behavior of the response provided mainly in the dark. For example, at −1.3 V, the potential at which water electrolysis happens, J_{ph} was −2.2, and −7.7 mA cm^{-2} for PECs based on 8 and 12 μg cm^{-2} of Ni co-catalyst loading, respectively, and −8.1 mA cm^{-2} for the NiCu-based cell.

Figure 5a shows both the enthalpy and throughput efficiencies of the three PEC cells based on Ni and NiCu co-catalysts at the photocathode together with the values achieved with the bare PEC between OCP and −1.6 V. The enthalpy efficiency (orange lines) reached the maximum value in the bias-assisted region between −0.4 V and −0.6 V, whereas the throughput efficiency (blue line) increased as the bias voltage became larger, due to an enhancement of the overall photocurrent at high bias voltages. Calculating the throughput efficiency for a tandem cell is the same as in a conventional (dark) electrolyzer, where the total energy output is divided by the total energy input.

The bare PEC without co-catalysts (Figure 5a) provided lower enthalpic and throughput efficiency in the same voltage range. In the case of Ni (8 μg cm^{-2}), Figure 5b shows a maximum enthalpic efficiency lower than 2% at about −0.5 V, and the throughput efficiency was about 3% at the same voltage. The best-performing PEC, in terms of efficiencies in the potential range of interest, was displayed in Figure 5c with Ni (12 μg cm^{-2}), followed by the PEC with NiCu (8 μg cm^{-2}) at the photocathode.

Table 1 summarizes data of the photocurrent (J_{ph}), enthalpy (η_{enth}), and throughput ($\eta_{throughput}$) efficiencies for the best-performing cell, where a 12 μg cm^{-2} Ni co-catalyst (Figure 5c) was added to the hydrophobized CuO/GDL photocathode. J_{ph} increases from 1.73 to 7.33 mA cm^{-2} in the potential range from −0.4 V to −1.225 V, corresponding to a growing difference between the current density values under illumination and in the dark. The enthalpy efficiency at −0.4 V reaches a maximum value of 2.03% and then decreases to

1.89% at -0.6 V as a result of the balance between the larger photocurrent and lower bias potential (E_{bias}).
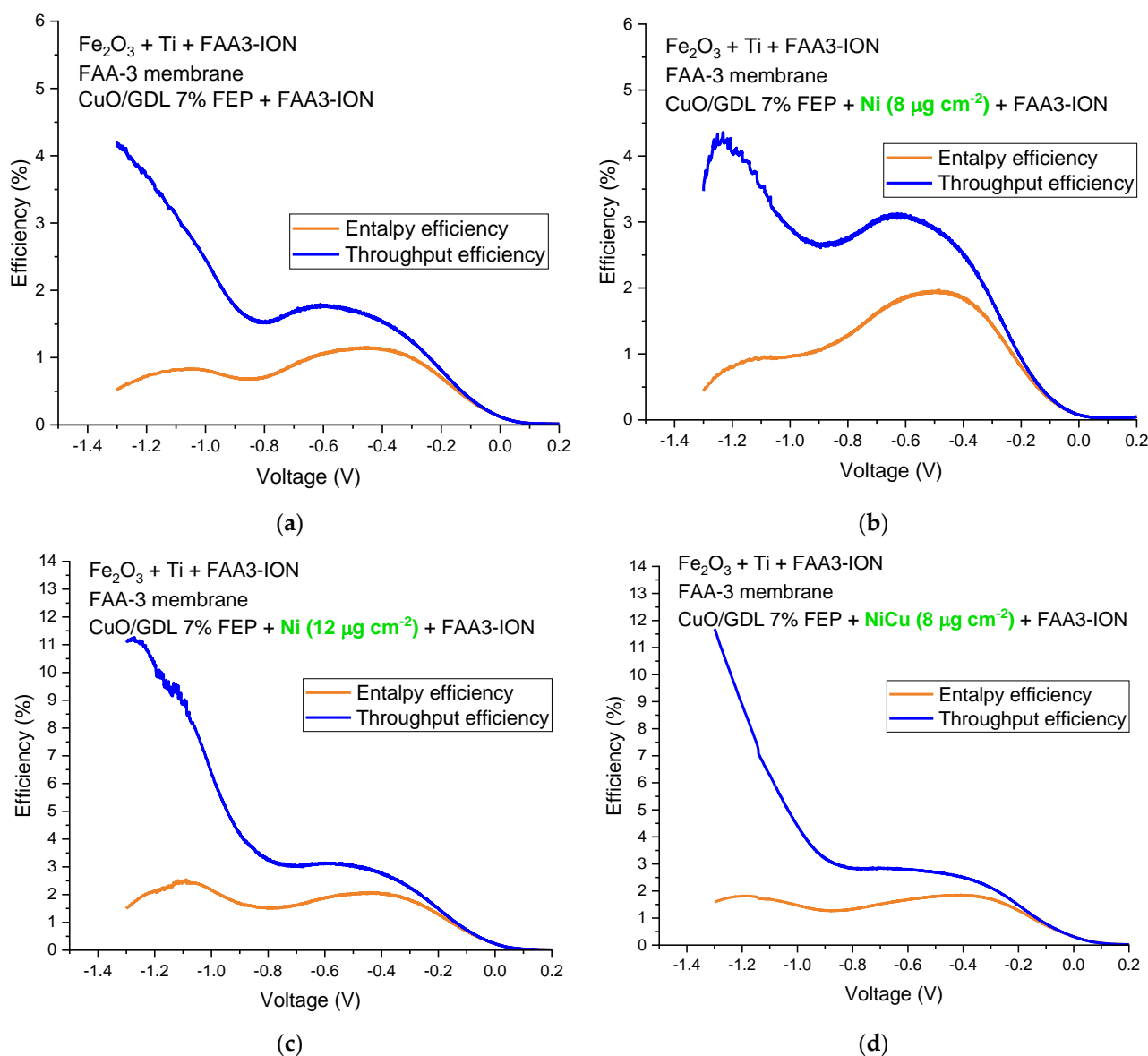
Figure 5. Enthalpy and throughput efficiency of PECs with photocathode co-catalyst loading: (**a**) bare PEC, (**b**) Ni ($8 \, \mu g \, cm^{-2}$), (**c**) Ni ($12 \, \mu g \, cm^{-2}$), and (**d**) NiCu ($8 \, \mu g \, cm^{-2}$). Bias is reported as the cathode potential minus the anode potential.

Table 1. Photocurrent density (J_{ph}), enthalpy efficiency (η_{enth}), and throughput efficiency ($\eta_{throughput}$) achieved by the addition of Ni co-catalyst to the photocathode.

V_{bias} (V)	J_{ph} (mA cm^{-2})	η_{enth} (%)	$\eta_{throughput}$ (%)
-0.4	1.73	2.03	2.76
-0.6	1.97	1.89	3.13
-1.225	7.33	2.03	10.75

The throughput efficiency is a ratio between the power output and the overall power input (solar + electric) supplied by an external source; thus, it increases in the function of a larger J_{ph}, and it achieves a maximum calculated at -1.225 V of 10.75%. This result is

three times higher than the best results obtained in our previous study with PEC cells in which co-catalysts were added at the photoanode.

Impedance spectra were performed in the bias-assisted region at -0.6 V under illumination to evaluate the kinetic and electrochemical effect of the PEC with a Ni or NiCu addition to the photocathode in comparison with a bare PEC. As evidenced by Figure 6, the value of charge transfer resistance is higher for the cell without co-catalysts, followed by the NiCu-based PEC and the Ni-based PEC. According to polarization curves and the calculated efficiencies, the addition of Ni and NiCu improves the charge transport and the photoelectrochemical activity of the overall photoelectrochemical cell.
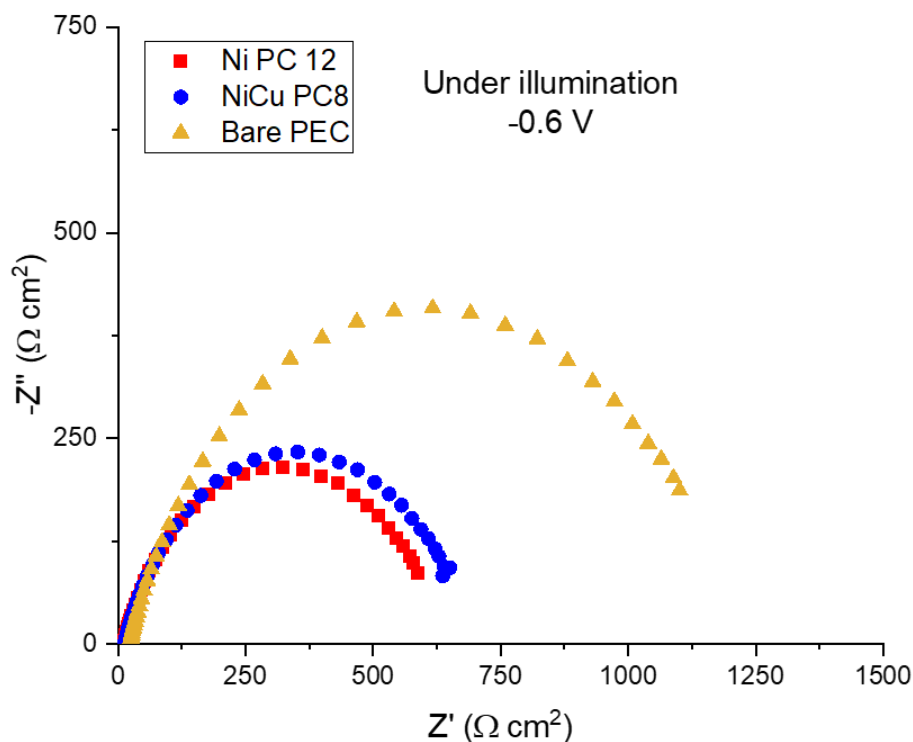

Figure 6. Impedance spectra for Ni- or NiCu-based PEC in comparison with the bare cell.

3. Materials and Methods

3.1. Synthesis of Photoelectrodes

3.1.1. Preparation of (110) Oriented Hematite Nanorods as Photoanodes

Hematite-based photoanodes were prepared as reported in our previous studies [34]. Briefly, the synthesis consists of a chemical bath deposition procedure followed by a thermal treatment. A transparent conductive oxide (TCO) glass substrate was vertically arranged in a solution containing 0.15 mol·L^{-1} FeCl$_3$·6H$_2$O (Sigma-Aldrich, St. Louis, MO, USA, 99%) and 1 M NaNO$_3$ (Sigma-Aldrich, 99%), treated at 100 °C for 6 h and dried in air (FeOOH/TCO). A final heat treatment at 650 °C for 1 h was performed to achieve hematite-based nanorods (α-Fe$_2$O$_3$/TCO).

3.1.2. Hematite Modification with Titanium and Phosphorus

The modification with Ti was achieved by dip-coating the FeOOH/TCO electrode in a solution 0.1 mol·L^{-1} of Ti-isopropoxide in isopropanol. The electrode was immersed and kept in the solution for 1 min using immersion and withdrawal rates of 450 mm/min. After coating, electrodes were dried at 100 °C for 30 min and then thermally annealed at 650 °C for 1 h in air. This treatment leads to a Ti-doped α-Fe$_2$O$_3$/TCO.

Ti-doped α-Fe$_2$O$_3$/TCO electrode was modified with P by dip-coating into a 0.1 mol·L^{-1} NH$_4$NaHPO$_4$ (Sigma-Aldrich, 99%) aqueous solution. Immersion and withdrawal cycles

of 1 min were performed at a rate of 450 mm/min. After coating, the electrodes were dried at 100 °C for 30 min and then thermally annealed for 30 min in air at 450 °C.

3.1.3. Preparation of Cupric Oxide onto Sigracet Gas Diffusion Layer (GDL) as a Photocathode

The optimized procedure to obtain CuO/GDL is detailed in our previous work [18]. First, CuO was prepared according to the oxalate method described in a patent [35] and thermally treated at 350 °C for 2 h allowing the CuO_X nanoparticle formation. In a subsequent step, the formation of metallic Cu was achieved by the reduction of the powder in a 10% H_2–90% N_2 atmosphere at 200 °C. Simultaneously, a backing layer of the GDL was hydrophobized for 5 min with a 1:1 v.v. Fluoro-Ethylene-Propylene (FEP):H_2O solution. Thus, metallic Cu was dispersed in isopropyl alcohol under sonication for half an hour and then sprayed with an airbrush (high-performance HP-CPlus from IWATA) onto hydrophobized GDL (Sigracet 39BC) until reaching a total load of 2.0 mg/cm^2 of metallic Cu. After spray-deposition, the Cu/GDL was washed with deionized water, and chemical oxidation was performed by immersion in 2.5 mol·L^{-1} aqueous solution of sodium hydroxide (NaOH, Scharlab, extra pure) and 0.125 mol·L^{-1} ammonium persulfate ($(NH_4)_2S_2O_8$, Sigma-Aldrich, 98%) for 11 min. Finally, the electrode was thermally treated in air at 300 °C for 1 h. The intermediate step of metallic copper formation led to an even deposition of the metal over the GDL substrate and, in general, good adhesion of the semiconductor on the backing layer.

3.1.4. Synthesis of Co-Catalysts for the Photocathode

The raw catalysts, consisting of NiOx and NiCuOx, were prepared by the oxalate method [35]. Ni and Cu nitrates were dissolved in distilled water and mixed with a solution of oxalic acid neutralized at pH 6.5 with NaOH. A molar ratio of 10 was adopted between the chelating agent and the metal. The formed complex was treated at 80 °C with H_2O_2 until precipitate formation occurred. The precipitate was filtered from the solution, washed, and dried at 100 °C for 24 h. It was then calcined at 350 °C for 120 min. This last thermal annealing led to the formation of NiOx or NiCuOx when a Cu precursor was employed. Thus, metallic Ni was obtained by reducing the corresponding oxide at 400 °C for 1 h and NiCu by reducing NiCuOx at 300 °C for 1 h both in a 5 mL/min H_2 + 95 mL/min N_2 environment. The catalytic inks were prepared by sonicating the co-catalyst powder with 2-propanol for half an hour in order to obtain a 2 mg mL^{-1} dispersion. Afterward, 8 and 12 µg cm^{-2} promoter loadings were collected and deposited on the CuO/GDL electrode using a doctor blade technique. Finally, the photocathode was subjected to a second heat treatment at 300 °C for 1 h before ionomer deposition.

3.1.5. Ionomer Preparation

The ionomer dispersion was prepared by solubilizing the received solid ionomer powder (FAA3-shredded film) in a mixture of solvents. An alcoholic solution of n-propanol and ethanol (1:1 wt) was used for this purpose, and the FAA3 ionomer was solubilized at room temperature under stirring to have ~5 wt% dispersion.

3.2. Assembly of the Photoelectrochemical Cell

Each of the four photoelectrochemical cells assembled with clamps for this work has a geometric area of 1 cm^2, with an active area of 0.25 cm^2. An anion exchange Fumasep membrane (FumaTech, Bietigheim-Bissingen, Germany), with a geometric area of 1.1 × 1.1 cm^2, was based on a polysulfone backbone and aminated functional groups; it was subjected to an anion-exchange process in 1 M KOH aqueous solution for 24 h before assembly to exchange the chloride by hydroxide. The FAA3 ionomer dispersion was deposited on both the photoanode (PA) and photocathode (PC) surfaces at 25 µL cm^{-2} ionomer loading (FAA3, 5 wt% in 1:1 ethanol-n-propanol mixture).

Ti-and-P-doped hematite, Ni- or NiCu-based PC, and the hydrated membrane were then brought into contact according to the following arrangement: photoanode/ionomer/

membrane/ionomer/photocathode. Before the cell assembly, the membrane and photo-electrodes were soaked in pure water, thus providing the necessary water content for the photoelectrochemical reaction. To insulate the back side of the hematite electrode, a black insulating tape was used so that the photoactive area was 0.25 cm^2.

Finally, the assembled cell was clamped with two paper clips for each side to provide sufficient pressure to secure all of the cell components. The PEC cell was tested in a solar simulator (Oriel) in a vertical position at 1.5 AM, corresponding to a power density of 92 mW cm^{-2}, as measured by a calibrated photovoltaic cell.

3.3. Physicochemical Characterization

X-ray diffraction (XRD) patterns for powder co-catalysts were acquired with an X'Pert 3710 X-Ray (Philips, Eindhoven, The Netherlands) diffractometer using a Cu-Kα source operating at 40 kV and 20 mA. The peak profiles of the X-ray reflections were obtained by applying the Marquardt algorithm to calculate the crystallite size by means of the Debye–Scherrer equation. The morphology of the co-catalysts was studied by scanning electron microscopy (SEM) with an FEI-XL 30 SEM microscope.

3.4. Electrochemical Tests

Working and sensing electrodes (WE, SE) were connected to the conductive part of FTO at the photoanode; reference and counter electrodes (RE, CE) were connected to the CuO-free GDL at the photocathode.

Polarization tests were carried out by sweeping the potential between the open circuit potential (OCP) value up to a bias of -1.3 V. Some graphs were reported in the region of interest (avoiding drastic conditions for degradation) up to -0.6 V (bias-controlled region) and recording the current density of the PEC first in the dark and thereafter under illumination. The sign of the recorded photocurrent and the potential bias are reported as negative (reverse current and applied bias) as in the case of photodiode mode. When a spontaneous photovoltage is recorded, it takes a positive sign, as is the case for the photodiode. The photocurrent measured between the OCP and the short circuit (i.e., 0 V) is driven by illumination only (spontaneous photocurrent); in this region, the potential is positive, whereas, in the negative potential region, an external bias-assisted photocurrent occurs.

Impedance spectra were carried out at a bias of -0.6 V under illumination for the best-performing electrochemical cell with and without the addition of co-catalysts. Frequency was varied from 1 KHz to 0.1 Hz (10 mVrms) with a frequency response analyzer (FRA) supported on Metrohm Autolab potentiostat/galvanostat.

3.5. Efficiency of the PEC

The efficiencies of photoelectrochemical cells were calculated as reported in Equations (1)–(3) and in previous papers [17–19,36,37].

$$\text{Enthalpy efficiency: } \eta = \text{Iph } (\Delta H/nF - \text{Ebias})/\text{Pin} = \text{Iph } (\text{Etn} - \text{Ebias})/\text{Pin} \qquad (1)$$

$$\text{Free energy efficiency: } \eta = \text{Iph } (\Delta G/nF - \text{Ebias})/\text{Pin} = \text{Iph } (\text{Erev} - \text{Ebias})/\text{Pin} \qquad (2)$$

$$\text{Throughput efficiency: } \eta = \text{Iph } (\Delta H/nF)/(\text{Pin} + \text{Iph Ebias}) = \text{Iph Etn}/(\text{Pin} + \text{Iph Ebias}) \qquad (3)$$

where Etn = 1.48 V, Erev = 1.23 V, Ebias $\equiv$ V, Pin $\equiv \text{mW cm}^{-2}$, and Iph = I light $-$ I dark $\equiv \text{mA cm}^{-2}$.

4. Conclusions

A small amount of homemade Ni-based co-catalysts were deposited onto a CuO/GDL-based photocathode of a photoelectrochemical cell formed using Ti-and-P-doped hematite photoanodes and an anionic exchange membrane used as a gas separator between oxygen and hydrogen evolution from photoelectrochemical water splitting. By comparing bare PEC with those obtained with 12 ug cm^{-2} of Ni co-catalysts, it appears that the use of

the co-catalyst promotes hydrogen evolution under illumination with the achievement of 10.75% in throughput efficiency at -1.225 V. At -0.6 V, the photocurrent density reaches approximately 2 mA cm^{-2} for the cell based on 12 μg cm^{-2} of Ni loading followed by 1.75 mA cm^{-2} for that based on 8 μg cm^{-2} of NiCu. For the best-performing cell, enthalpy efficiency at -0.4 V reaches a maximum value of 2.03%. Interestingly, these co-catalysts can be loaded directly on the photocathode material, without the need for the previous deposition of a buffer layer. This simplifies the electrode modification and favors its viability.

The scalability of such a kind of PEC could enhance the production of hydrogen for possible future applications for green technology.

Author Contributions: Conceptualization, R.G. and A.S.A.; methodology, A.S.A., R.G. and V.B.; synthesis, M.I.D.-G., M.C. and C.L.V.; investigation, C.L.V., S.T., G.G. and O.B.; data curation, C.L.V., S.T., G.G. and O.B.; writing—original draft preparation, C.L.V.; writing—review and editing, V.B., A.S.A., R.G., M.C. and M.I.D.-G. All authors have read and agreed to the published version of the manuscript.

Data Availability Statement: The data presented in this study are available on request from the corresponding author.

Conflicts of Interest: The authors declare no conflict of interest.

References

1. Romprasert, S. Energy risk with community management and cost analysis. *Int. J. Manag.* **2020**, *11*, 1136–1144. [CrossRef]
2. Chen, S.; Kharrazi, A.; Liang, S.; Fath, B.D.; Lenzen, M.; Yan, J. Advanced approaches and applications of energy footprints toward the promotion of global sustainability. *Appl. Energy* **2020**, *261*, 114415. [CrossRef]
3. Rabaia, M.K.H.; Abdelkareem, M.A.; Sayed, E.T.; Elsaid, K.; Chae, K.; Wilberforce, T.; Olabi, A.G. Environmental impacts of solar energy systems: A review. *Sci. Total Environ.* **2021**, *754*, 141989. [CrossRef]
4. Wu, Y.; Li, C.; Tian, Z.; Sun, J. Solar-driven integrated energy systems: State of the art and challenges. *J. Power Sources* **2020**, *478*, 228762. [CrossRef]
5. Dhar, A.; Naeth, M.A.; Jennings, P.D.; El-Din, M.G. Perspectives on environmental impacts and a land reclamation strategy for solar and wind energy systems. *Sci. Total Environ.* **2020**, *718*, 134602. [CrossRef] [PubMed]
6. Gratzel, M. Photoelectrochemical cells. *Nature* **2001**, *414*, 338–344. [CrossRef] [PubMed]
7. Khaselev, O.; Turner, J.A. A monolithic photovoltaic-photoelectrochemical device for hydrogen production via water splitting. *Science* **1998**, *280*, 425–428. [CrossRef]
8. Bak, T.; Nowotny, J.; Rekas, M.; Sorrell, C.C. Photo-electrochemical hydrogen generation from water using solar energy. Materials-related aspects. *Int. J. Hydrog. Energy* **2002**, *27*, 991–1022. [CrossRef]
9. Fujishima, A.; Honda, K. Electrochemical photolysis of water at a semiconductor electrode. *Nature* **1972**, *238*, 37–38. [CrossRef]
10. Silva, A.B.; Da Silva, C.D.F.; Souza, F.L.; Lucas, F.W.S.; Lima, F.H.B. All-electrochemically synthesized tin and nickel oxide-modified hematite as photo-electrocatalyst anodes for solar-driven water splitting. *J. Cat.* **2020**, *391*, 273–281. [CrossRef]
11. Deshmukh, P.R.; Sohn, Y.; Shin, W.G. Chemical synthesis of ZnO nanorods: Investigations of electrochemical performance and photo-electrochemical water splitting applications. *J. Alloy. Comp.* **2017**, *711*, 573–580. [CrossRef]
12. English, N.J. Electric-field-promoted photo-electrochemical production of hydrogen from water splitting. *J. Mol. Liq.* **2021**, *342*, 116949. [CrossRef]
13. Chaudhary, P.; Ingole, P.P. Nickel incorporated graphitic carbon nitride supported copper sulfide for efficient noble-metal-free photo-electrochemical water splitting. *Electrochim. Acta* **2020**, *357*, 136798. [CrossRef]
14. Rani, D.S.; Meera, M.R. Photo-electrochemical water splitting behavior of CdSeQDs sensitized ferroelectric BaTiO3 perovskite heterostructure. *Mater. Today* **2020**, *37*, 1248–1253. [CrossRef]
15. Aricò, A.S.; Girolamo, M.; Siracusano, S.; Sebastian, D.; Baglio, V.; Schuster, M. Polymer Electrolyte Membranes for Water Photo-Electrolysis. *Membranes* **2017**, *7*, 25. [CrossRef] [PubMed]
16. Cots, A.; Bonete, P.; Sebastian, D.; Baglio, V.; Aricò, A.S.; Gomez, R. Toward tandem solar cells for water splitting using polymer electrolytes. *ACS Appl. Mater. Interfaces* **2018**, *10*, 25393–25400. [CrossRef]
17. Vecchio, C.L.; Trocino, S.; Zignani, S.C.; Baglio, V.; Carbone, A.; Garcia, M.I.D.; Contreras, M.; Gómez, R.; Aricò, A.S. Enhanced PhotoelectrochemicalWater Splitting at Hematite Photoanodes by Effect of a NiFe-Oxide co-Catalyst. *Catalysts* **2020**, *10*, 525. [CrossRef]

18. Trocino, S.; Vecchio, C.; Lo Zignani, S.C.; Carbone, A.; Saccà, A.; Baglio, V.; Gòmez, R.; Aricò, A.S. Dry Hydrogen Production in a Tandem Critical Raw Material-FreeWater Photoelectrolysis Cell Using a Hydrophobic Gas-Diffusion Backing Layer. *Catalysts* **2020**, *10*, 1319. [CrossRef]

19. Lo Vecchio, C.; Carbone, A.; Trocino, S.; Gatto, I.; Patti, A.; Baglio, V.; Aricò, A.S. Anionic Exchange Membrane for Photo-Electrolysis Application. *Polymers* **2020**, *12*, 2991. [CrossRef] [PubMed]

20. Sivula, K.; Le Formal, F.; Grätzel, M. Solar Water Splitting: Progress Using Hematite (α-Fe_2O_3) Photoelectrodes. *ChemSusChem* **2011**, *4*, 432–449. [CrossRef]

21. Burton, N.A.; Padilla, R.V.; Rose, A.; Habibullah, H. Increasing the efficiency of hydrogen production from solar powered water electrolysis. *Renew. Sustain. Energy Rev.* **2021**, *135*, 110255. [CrossRef]

22. La Ganga, G.; Mollica Nardo, V.; Cordaro, M.; Natali, M.; Vitale, S.; Licciardello, A.; Nastasi, F.; Campagna, S. A functionalized, ethynyl-decorated, tetracobalt(III) cubane molecular catalyst for photoinduced water oxidation. *Dalton Trans.* **2014**, *43*, 14926. [CrossRef] [PubMed]

23. Berger, A.; Segalman, R.A.; Newman, J. Material requirements for membrane separators in a water-splitting photoelectrochemical cell. *Energy Environ. Sci.* **2014**, *7*, 1468–1476. [CrossRef]

24. Hsu, Y.-K.; Yu, C.-H.; Lin, H.-H.; Chen, Y.-C.; Lin, Y.-G. Template synthesis of copper oxide nanowires for photoelectrochemical hydrogen generation. *J. Electroanal. Chem.* **2013**, *704*, 19–23. [CrossRef]

25. Kment, Š.; Sivula, K.; Naldoni, A.; Sarmah, S.P.; Kmentov, H.; Kulkarni, M.; Rambabu, Y.; Schmuki, P.; Zboril, R. FeO-based nanostructures and nanohybrids for photoelectrochemical water splitting. *Prog. Mater. Sci.* **2020**, *110*, 100632. [CrossRef]

26. Adamopoulos, P.M.; Papagiannis, I.; Raptis, D. Photoelectrocatalytic Hydrogen Production Using a TiO_2/WO_3 Bilayer Photocatalyst in the Presence of. Ethanol as a fuel. *Catalysts* **2019**, *9*, 976. [CrossRef]

27. Carbone, A.; Pedicini, R.; Gatto, I.; Saccà, A.; Patti, A.; Bella, G.; Cordaro, M. Development of Polymeric Membranes Based on Quaternized Polysulfones for AMFC Applications. *Polymers* **2020**, *12*, 283. [CrossRef] [PubMed]

28. Carbone, A.; Zignani, S.C.; Gatto, I.; Trocino, S.; Aricò, A.S. Assessment of the FAA3-50 polymer electrolyte in combination with a $NiMn_2O_4$ anode catalyst for anion exchange membrane water electrolysis. *Int. J. Hydrog. Energy* **2020**, *45*, 9285–9292. [CrossRef]

29. Varcoe, J.R.; Atanassov, P.; Dekel, D.R.; Herring, A.M.; Hickner, M.A.; Kohl, P.A.; Kucernak, A.R.; Mustain, W.E.; Nijmeijer, K.; Scott, K.; et al. Anion-exchange membranes in electrochemical energy systems. *Energy Environ. Sci.* **2014**, *7*, 3135–3191. [CrossRef]

30. Li, X.; Liu, A.; Chu, D.; Zhang, C.; Du, Y.; Huang, J.; Yang, P. High Performance of Manganese Porphyrin Sensitized p-Type $CuFe_2O_4$ Photocathode for Solar Water Splitting to Produce Hydrogen in a Tandem Photoelectrochemical Cell. *Catalysts* **2018**, *8*, 108. [CrossRef]

31. Jing, S.; Yin, D.S.; Lu, J.; Shen, P.K.; Tsiakaras, P. P-doped CNTs encapsulated nickel hybrids with flower-like structure as efficient catalysts for hydrogen evolution reaction. *Electrochim. Acta* **2019**, *298*, 6582–6591. [CrossRef]

32. Sim, Y.; John, J.; Moon, J.; Sim, U. Photo-Assisted Hydrogen Evolution with Reduced Graphene Oxide Catalyst on Silicon Nanowire Photocathode. *Appl. Sci.* **2018**, *8*, 2046. [CrossRef]

33. Cots, A.; Bonete, P.; Gomez, R. Improving the stability and efficiency of CuO photocathodes for solar hydrogen production through modification with iron. *ACS Appl. Mater. Interfaces* **2018**, *10*, 26348–26356. [CrossRef]

34. Cots, A.; Cibrev, D.; Bonete, P.; Gomez, R. Hematite nanorod electrodes modified with molybdenum: Photoelectrochemical studies. *ChemElectroChem* **2017**, *4*, 585–593. [CrossRef]

35. Aricò, A.S.; Gullo, L.R.; La Rosa, D.; Diracusano, S.; Tavares, A.B.L.C.; Xicola, A.S. Solid Oxide Fuel Cell with Cermet Cu/Ni Alloy Anode. *Patent WO* **2004**, *49491*, 10.

36. Tsotridis, G.; Pilenga, A. *JRC Technical Reports "EU Harmonised Terminology for Low-Temperature Water Electrolysis for Energy-Storage Applications"*; Publications Office of the European Union: Brussels, Belgium, 2018; pp. 1–90.

37. Chen, Z.; Dinh, H.N.; Miller, E. *Photoelectrochemical Water Splitting Standards, Experimental Methods and Protocols*; Springer: New York, NY, USA, 2013.